
# Final Draft

## of the original manuscript

Jiang, P.; Blawert, C.; Scharnagl, N.; Zheludkevich, M.L.:

**Influence of water purity on the corrosion behavior of Mg0.5ZnX (X=Ca, Ge) alloys.**

In: Corrosion Science. Vol. 153 (2019) 62 - 73.
First published online by Elsevier: 28.03.2019

https://dx.doi.org/10.1016/j.corsci.2019.03.044

# Influence of water purity on the corrosion behavior of Mg0.5ZnX (X=Ca, Ge) alloys

Pingli Jiang[a*], Carsten Blawert[a], Nico Scharnagl[a], Mikhail L. Zheludkevich[a,b]

[a] Magnesium Innovation Centre - MagIC, Institute of Materials Research, Helmholtz-Zentrum Geesthacht, Max-Planck Str.1, Geesthacht 21502, Germany

[b] Faculty of Engineering, University of Kiel, Kaiserstrasse 2, 24143 Kiel, Germany

[*] Corresponding author:

Pingli Jiang, Phone: +49 (0)4152 871936, E-mail: *pingli.jiang@hzg.de*

**Abstract**

Influence of water purity on the corrosion behavior of as-cast Mg0.5Zn, Mg0.5Zn0.5Ca and Mg0.5Zn0.2Ge alloys was investigated by preparing 0.9 *wt.*% NaCl solution with deionized and tap water. $Mg(OH)_2$ layer with limited protection ability was predominately formed on the surfaces in solution prepared with deionized water. In contrast, besides the primary $Mg(OH)_2$ layer, different crystals of $CaCO_3$ were formed as a secondary corrosion products layer in solution prepared with tap water, which improved the corrosion resistance of alloys by almost one order of magnitude. Moreover, the crystallographic form of $CaCO_3$ was influenced by the content of calcium in the alloy.

Keywords: Magnesium; Water purity; Corrosion; Calcium carbonate.

## 1. Introduction

In recent decades, magnesium (Mg) and its alloys have been extensively studied for their applications in aircraft, aeronautical, automobile and electronic industries [1]. With a low density of 1.74 g $cm^{-3}$, Mg is the lightest engineering structural metal, which is important for the aim of saving energy and fuels, reducing carbon dioxide ($CO_2$) emissions and designing portable electronics [1, 2]. Besides, the high specific strength, good castability, weldability and machinability also contribute to their increasing industrial applications [3]. Since the galvanic potential of Mg in aqueous electrolytes is the most negative among all engineering metallic materials, severe corrosion attack often occurs to Mg assemblies in aqueous environment, which has long been a major obstacle for the widespread structural applications of Mg and its alloys [4]. Therefore, a comprehensive understanding of the corrosion behavior of Mg and its alloys is of considerable importance.

Usually, the corrosion behavior of Mg alloys is significantly affected by their surroundings [5]. Plenty of work has been carried out to understand individual or mutual influences of anions or cations in simulated service environments, such as $Cl^-$, $HCO_3^-$, $SO_4^{2-}$ and $Ca^{2+}$ etc. [6-12]. In general, it is widely accepted that $Cl^-$ can promote the dissolution of Mg alloys in aqueous solutions [5, 13]. $SO_4^{2-}$ is also believed to stimulate Mg dissolution but not as severe as $Cl^-$ [9, 14]. $HCO_3^-$ can accelerate the overall corrosion rate of Mg alloy but can also induce rapid surface passivation and subsequently suppress pitting corrosion [8, 9]. Individual presence of $Ca^{2+}$ cannot obviously influence the corrosion behavior of Mg alloys in solution of sodium chloride (NaCl). However, when $Ca^{2+}$ are present together with $HPO_4^{2-}$ and/or $HCO_3^-$, they can increase the general corrosion resistance of Mg alloy due to the formation of a protective surface film [8]. Corrosion behavior of Mg alloys under various simulated surroundings, such as simple NaCl solutions at different concentrations [15, 16], 3.5 *wt.*% NaCl solution saturated with magnesium hydroxide ($Mg(OH)_2$) [17, 18] and artificial

seawater [19] etc., has been widely reported. Nevertheless, few studies were carried out to investigate the corrosion behavior of Mg alloys in tap water or the influence induced by water purity on the corrosion resistance of Mg alloys.

Therefore, in this study, the influence induced by water purity was investigated by studying the corrosion behavior of Mg0.5ZnX alloys in a corrosive solution prepared with deionized water and tap water. Natural instead of artificial tap water was boldly and directly used to have a direct understanding of the influence of water purity. In order to avoid the overwhelming effect generated by those substances apart from the water, the simplest physiological saline (0.9 *wt.*% NaCl) was used to provide a corrosive environment. Mg-Zn based alloys were selected because Mg-Zn system has attracted increasing attention for both industrial and biomedical applications recently, especially in biomedical material field [20-22]. Therefore, Mg0.5Zn, Mg0.5Zn0.5Ca and Mg0.5Zn0.2Ge alloys were used in the present study. Two Mg-Zn alloys with a trace Ca content (one of them with Ge as ternary alloying element) and one with 0.5 *wt.*% Ca were tested to study the possible influence induced by Ca contained in the bulk material and the influence of Ca in the water.

## 2. Experimental

### 2.1. Materials

The nominal Mg0.5Zn, Mg0.5Zn0.5Ca and Mg0.5Zn0.2Ge alloys in weight percentage were prepared from pure Mg (99.96 %), Zn (99.995 %), Ca (99.9 %) and/or Ge (99.99 %) using an electric furnace under a protective atmosphere of Ar and $SF_6$ at 760 $^{\circ}$C. The melts were stirred for 5 minutes and then casted into a steel mold preheated to 200 $^{\circ}$C. Cylindrical specimens in a size of Φ 18 mm × 6 mm were cut from the alloy bars and then wet ground with silicon paper from 800 to 1200 grid for corrosion and electrochemical tests. Spark optical emission spectroscopy (Spectrolab M9 Kleve, Specro Ametek, Germany) was adopted to analyze the

chemical compositions of the alloys, as listed in Table 1. The content of Ge in Mg0.5Zn0.2Ge alloy was tested by micro X-ray Fluorescence (μXRF) (M4 TRONADO, Bruker, Germany).

2.2. Solution preparation

The tap water is supplied by the local 'Wasserwerk Krümmel' and the deionized water is produced by a standard membrane-based reverse-osmosis (RO) system. The composition of the deionized water (RO) and tap water is summarized in Table 2. The conductivity and pH were determined with a conductivity meter (S47 SevenMulti, Mettler-Toledo GmbH, Schweiz,) and a pH meter (713 pH meter, Metrohm AG, Switzerland), respectively. Obviously, the most important difference is the conductivity, hardness and Ca content. 0.9 *wt.*% NaCl (AR Grade) solution was prepared with tap water and deionized water, respectively.

2.3. Electrochemical measurements

The corrosion behavior of all alloys was evaluated by potentiodynamic polarization and electrochemical impedance spectroscopy (EIS) measurements. All electrochemical tests were performed with a Gill AC potentiostat/frequency response analyzer system (Gill AC, ACM Instruments, United Kingdom). A conventional three-electrode cell was used, in which the working electrode is Mg alloy samples, the reference electrode is an Ag/AgCl electrode (with saturated potassium chloride solution) and the counter electrode is a platinum mesh. The exposed area of samples was 0.5 $cm^2$. The electrochemical tests were carried out in 0.9 *wt.*% NaCl solution prepared with tap or deionized water, respectively, under atmospheric conditions at room temperature (air-conditioned at about 21 $^{\circ}C$) with magnetic stirring at a speed of 200 r/min. EIS measurements were conducted with the frequency range of 30000 - 0.1 Hz and an AC voltage amplitude of 10 mV rms at open circuit potential (OCP). The impedance spectra were collected after immersion for different durations to monitor the

development of the corrosion resistance with exposure time. Zview software was used to fit the impedance spectra. Potentiodynamic polarization tests were conducted from -0.15 to 0.7 V vs. OCP at a scanning rate of 0.2 mV $s^{-1}$ after 7 d of immersion in 0.9 *wt.*% NaCl solution. The intercept corrosion rate (*CR*) and corrosion current density ($i_{corr}$) were analyzed with ACM Analysis software by selecting the linear part of the cathodic curve that commenced about 50 mV from corrosion potential ($E_{corr}$), and subsequently *CR* and $i_{corr}$ were estimated from the value where the fit intercepted the vertical through the true $E_{corr}$ value [24]. Note that, only the cathodic part was used for the fitting. All electrochemical measurements were repeated for at least four times for statistical purpose.

2.4. Analysis of corrosion morphologies and products

To investigate the influence of water purity on the corrosion morphologies and products on different Mg0.5ZnX alloys, immersion tests were conducted in 0.9 *wt.*% NaCl solution prepared with tap or deionized water for 7 d.

The surfaces after immersion were examined by X-ray diffraction (XRD) with a diffractometer (D8 Advance, Bruker, Germany) in grazing incidence geometry at an incidence angle of 3° to identify the composition of the corrosion products formed in different solutions. The measurements were performed at 40 kV and 40 mA with a step size of 0.02° and 1 s for each step from $2\theta = 5^{\circ}$ to 85°. The data was analyzed by using Bruker EVA software with PDF-2 Release 2015 RDB. The corroded surfaces were also examined by using an X-ray photoelectron spectrometer (XPS) (Kratos Axis Ultra DLD, Kratos Analytical, United Kingdom) which is equipped with a monochromatic Al Kα anode. The working voltage is 15 kV (225 W). The investigated area was 700 μm × 300 μm. The pass energy for survey spectra and region spectra measurements was 160 eV and 20 eV, respectively. Ar etching was performed for depth profiling at a rate of 10 nm/min related to $Ta_2O_5$. During Ar etching, the acceleration voltage and extraction current were 3.8 kV and 160 mA,

respectively. For all specimens, it was necessary to do charge neutralization. The data was evaluated and validated with CASA-XPS software (version 2.3.18). The C 1s signal was adjusted to 284.5 eV to calibrate the spectra. Background subtraction was carried out before calculation for deconvolution of the region spectra.

The surface morphologies of the specimens after immersion were examined by scanning electron microscopy (SEM) (Vega 3 SB, TESCAN Brno, Czech Republic) equipped with energy dispersive X-ray spectroscopy (EDS) system in backscattering (BSE) mode with an accelerating voltage of 20 kV.

The cross sections of the corroded morphologies were also checked with SEM by vertically mounting the corroded specimens in epoxy resin. All images were taken in BSE mode. Element mapping was carried out with EDS to determine the distribution of element in the corrosion product film. The resolution was 256 × 191 pixels and the acquisition time was 80 ms per pixel.

## 3. Results

### 3.1. Corrosion behavior

#### 3.1.1. Electrochemical impedance spectroscopy measurements

EIS is a powerful technique to detect the development of corrosion processes and follow the evolution of interfacial layers on metal surfaces during immersion in corrosive media. To investigate the influence induced by water purity on the corrosion behavior of Mg0.5ZnX alloys, EIS measurements were conducted for up to 7 d in 0.9 *wt.*% NaCl solutions prepared with deionized water and tap water.

Fig. 1 shows the impedance spectra of Mg0.5Zn, Mg0.5Zn0.5Ca and Mg0.5Zn0.2Ge alloys tested in 0.9 *wt.*% NaCl solution prepared with deionized water. The Nyquist plots of Mg0.5Zn (Fig. 1a) and Mg0.5Zn0.5Ca (Fig. 1d) alloys show two well-defined capacitive

semicircles, one in the high frequency area and another in the middle frequency area. In comparison, for Mg0.5Zn0.2Ge alloy (Fig. 1g), the capacitive loop at middle frequency is less defined than that in the cases of the other two alloys after immersion for more than 3 h. However, with continued immersion, the impedance spectrum develops as two well-defined capacitive loops again after 24 h. In solution prepared with tap water, the behavior is different. All of the Nyquist plots (Fig. 2a, 2d, 2g), irrespective of which alloy, exhibit two well-defined capacitive loops and the diameters of the loops are much larger than those tested in solution prepared with deionized water after immersion for more than 24 h. In addition, it is noted from the Bode plots (Fig. 2c, 2f, 2i) that a new time constant appears at high frequency region with prolonged immersion time and it is more obvious for Mg0.5Zn and Mg0.5Zn0.2Ge alloys, which should be ascribed to the generation of a new layer of corrosion products.

To further understand the evolution of the corrosion resistance of the three alloys in different corrosive media, the impedance spectra were fitted with two different equivalent circuits (Fig. 3) according to the characteristics of the spectra and the fitted data were plotted in Fig. 4. It can be clearly observed from the Bode plots in Fig 2c, 2f and 2i, in solution prepared with tap water, the charge transfer process was almost undistinguishable after 24 h. This was because of the gradually increased resistance resulting from the thicker and more compact corrosion product layers with extended immersion time, which were hiding the response of the double electric layer. Consequently, the accurate fitting for the double layer capacitance would be not possible. To avoid possible controversy, the detailed fitted parameters were not presented. In the equivalent circuits, $R_s$ is the solution resistance between the reference electrode and the working electrode. $R_{ct}$ accounts for the charge transfer resistance parallel to the double electric layer at the interface of the alloy and the electrolyte, $CPE_{dl}$. $R_{f1}$ and $CPE_{f1}$ represent the corrosion resistance and capacity of the primary corrosion product film. $R_{f2}$ and $CPE_{f2}$

were introduced to account for the secondary corrosion product layer in the case of solution prepared with tap water. The second equivalent circuit with three time constants was only used when the third relaxation process was evidenced at the spectra at high frequencies. In all other cases, the first equivalent consisting of two time constants was applied. For comparison, the sum ($R_{sum}$) of $R_{ct}$, $R_{f1}$ and $R_{f2}$ is displayed.

It can be seen from Fig 4a that $R_{sum}$ of Mg0.5Zn and Mg0.5Zn0.5Ca alloys fluctuated within immersion of up to 24 h and then gradually increased with prolonged immersion. In comparison, $R_{sum}$ of Mg0.5Zn0.2Ge alloy increased within the initial 3 h of immersion but then obviously dropped. After 24 h, $R_{sum}$ climbed again with increasing immersion time. Generally, the order of corrosion resistance of the three alloys in 0.9 *wt.*% NaCl solution prepared with deionized water is Mg0.5Zn > Mg0.5Zn0.5Ca > Mg0.5Zn0.2Ge. However, when the corrosive solution was prepared with tap water, $R_{sum}$ values (Fig. 4b) of all of the three alloys gradually increased with immersion time and were specifically higher than those measured in solution prepared with deionized water after 24 h. In addition, the corrosion resistance of Mg0.5Zn and Mg0.5Zn0.2Ge alloys was similar and higher than that of Mg0.5Zn0.5Ca alloy, especially after immersion for 24 h.

3.1.2. Potentiodynamic polarization analysis

Potentiodynamic polarization was also carried out for alloys after immersion in 0.9 *wt.*% NaCl solution prepared with deionized water and tap water for 7 d to examine the corrosion protective property of the corrosion product film formed in different medium, as shown in Fig. 5. Apparently, the corrosion current densities of alloys immersed in solution prepared with tap water are distinctly lower than those measured in solution prepared with deionized water. Meanwhile, all anodic curves exhibit an extended low-current plateau region, indicating that corrosion product films were formed on the alloy surfaces in solution prepared with both deionized and tap water and retarded the anodic dissolution of the alloys.

The fitted corrosion parameters are listed in Table 3. In solution prepared with deionized water, the results reveal that the corrosion resistance of alloys increase in the order of: Mg0.5Zn0.2Ge < Mg0.5Zn0.5Ca < Mg0.5Zn, which is consistent with the impedance results. Meanwhile, in the case of solution prepared with tap water, *CR* and $i_{corr}$ of Mg0.5Zn and Mg0.5Zn0.2Ge alloys were quite similar. In contrast, *CR* and $i_{corr}$ of Mg0.5Zn0.5Ca alloy were higher. This is in good agreement with the EIS results and suggests that the corrosion behavior of Mg0.5Zn and Mg0.5Zn0.2Ge alloys was similar in 0.9 *wt.*% NaCl solution prepared with tap water and the corrosion product films formed on the surfaces had similar properties and were more protective than that formed on the surface of Mg0.5Zn0.5Ca alloy. Notably, the *CR* and $i_{corr}$, irrespective of which alloy, decreased almost by one order of magnitude when the alloys were immersed in solution prepared with tap water. Thus, it can be concluded that the corrosion product films formed in solution prepared with tap water were much more protective to the alloys.

### 3.2. Corrosion product morphologies

As revealed by the EIS and potentiodynamic polarization results, the corrosion resistance of the studied alloys were much higher in NaCl solution prepared with tap water. Moreover, in solution prepared with tap water, the corrosion product films formed on the surfaces of Mg0.5Zn and Mg0.5Zn0.2Ge alloys were more protective than that formed on the surface of Mg0.5Zn0.5Ca alloy. Therefore, the surface and cross-sectional morphologies after corrosion were checked to understand the corrosion behavior of Mg0.5ZnX alloys under different corrosive environments better.

#### 3.2.1 Surface morphologies

Fig. 6 shows the surface morphologies of Mg0.5Zn, Mg0.5Zn0.5Ca and Mg0.5Zn0.2Ge alloys after 7 d of immersion in 0.9 *wt.*% NaCl solution prepared with deionized water.

Obviously, the corroded surface morphologies of the studied alloys were similar. The alloy surfaces were covered by cracked corrosion product films and the cracks were deeper and severer for Mg0.5Zn0.5Ca and Mg0.5Zn0.2Ge alloys, which may indicate that the films formed on the surfaces of Mg0.5Zn0.5Ca and Mg0.5Zn0.2Ge alloys were more hydrated [25] or had a higher thickness. In addition, a few aggregation of corrosion products formed and were randomly distributed on the cracked products layer (as indicated by the arrows).

When the alloys were immersed in NaCl solution prepared with tap water, totally different surface morphologies were formed. As shown in Fig. 7, regularly shaped cubic and flower-like products closely arranged on the surfaces of Mg0.5Zn and Mg0.5Zn0.2Ge alloys. Interestingly, a new pyramid-shape product was formed on the surface of Mg0.5Zn0.5Ca alloy and the flower-like product disappeared. In addition, the regularly shaped cubic and pyramid products were randomly distributed on the surface of Mg0.5Zn0.5Ca alloy and only partly covered the primary corrosion products layer.

3.2.2. Cross-sectional corrosion products morphologies

Fig. 8 displays the cross-sectional morphologies of Mg0.5Zn, Mg0.5Zn0.5Ca and Mg0.5Zn0.2Ge alloys after immersion in 0.9 *wt.*% NaCl solution prepared with deionized water and tap water for 7 d. The white lines on the resin were from the charging effects during imaging due to the poor conductivity of the resin. In NaCl solution prepared with deionized water, only one layer of corrosion products was observed and the thickness of the corrosion products film of Mg0.5Zn0.2Ge alloy was visually thicker than those of Mg0.5Zn and Mg0.5Zn0.5Ca alloys, indicating more serious corrosion of the Mg0.5Zn0.2Ge alloy during immersion, which is consistent with the EIS and potentiodynamic polarization results. However, in NaCl solution prepared with tap water, apparently, a new layer of corrosion products was formed besides the inner severely cracked layer. The outer layer completely covered the inner layer and was irregular in thickness for Mg0.5Zn and Mg0.5Zn0.2Ge alloys.

The irregular thickness of the outer layer is related to the different shape and size of the cubic and flower-like corrosion products. In accordance with the surface morphology, the outer layer of the corrosion product film of Mg0.5Zn0.5Ca alloy only partly covered the surface with some inner layer exposed.

To validate the chemical composition of the corrosion products formed in different corrosive media, element mapping was carried out for the cross sections of the three alloys after immersion in NaCl solution prepared with deionized and tap water, as presented in Fig. 9. The results were similar for different alloys and thus only the mappings for Mg0.5Zn alloy were presented as representative. As expected, the corrosion product film formed in NaCl solution prepared with deionized water was rich in oxygen (O) and Mg with little Ca and Zn. Interestingly, in the case of solution prepared with tap water, element distribution in the inner layer of the corrosion product film was similar to the case of deionized water, while the outer layer was extremely rich in Ca with some carbon (C) and O. In addition, Zn can also be found in the outer layer. According to the elemental mapping results, it can be speculated that the corrosion product film formed in solution prepared with deionized water and the inner layer of the film formed in NaCl solution prepared with tap water most likely is $MgO/Mg(OH)_2$, while the outer layer of the corrosion product formed in solution prepared with tap water may be $CaCO_3$ based.

### 3.3. Composition analysis of the corrosion products

XPS and XRD analysis were performed for the corroded surfaces to determine the detailed composition of the corrosion products formed in solutions prepared with deionized and tap water.

XPS can provide valuable information about the elements in the near surface. The XPS survey spectra (Fig. 10), with Mg0.5Zn alloy after immersion for 6 h as representative,

reveals the presence of Mg, C, O and Zn elements for sample immersed in solution prepared with deionized water. In the case of solution prepared with tap water, high intensity peak of Ca was detected. Additionally, the intensity of Mg 2s and Mg 2p decreased while that of C 1s increased significantly. Zn 2p was hardly detected in both of these two cases. High-resolution C 1s and Ca 2s region spectra are presented in Fig. 11. Owing to the strong overlap between the Auger Mg KLL peak and Ca 2p peak, the Ca 2s peak was evaluated instead [26]. Obviously, compared with the broad and low-intensity C 1s and Ca 2s spectra of specimen corroded in solution prepared with deionized water, those spectra in the case of tap water are highly centered, especially for the Ca 2s spectrum. The low-intensity C 1s spectrum of Mg0.5Zn alloy immersed in solution prepared with deionized water was fitted with five components (Fig. 11a). Among them, the binding energy (BE) peak at 289.04 eV can possibly be associated with carbon in -$CO_3$, which may be caused by the transformation from $Mg(OH)_2$ to magnesite ($MgCO_3$) due to the inevitable exposure to the air during the sample handling process (from frying to the sample chamber). While other peaks should be caused by the adventitious contamination (C-C/C-H carbon at about 284.75 eV, C-O carbon at around 286.86 eV, C=O carbon at about 287.78 eV and CO-type generated by oxygen contamination at around 290.75 eV) [27, 28]. The intensity of Ca 2s was too low to be fitted, indicating the low content of Ca element in the surface of Mg0.5Zn alloy after immersion in NaCl solution prepared with deionized water. For Mg0.5Zn alloy surface corroded in solution prepared with tap water, the C 1s composite peak was deconvoluted into two peaks corresponding to C-C/C-H carbon contamination at 284.11 eV and carbon present in the carbonate category at 289.45 eV [27, 29, 30]. Ca 2s was fitted with one component at 437.43 eV which corresponds to calcium associated with $CaCO_3$. Some BE shift can be found between different samples or between our results and published ones, which should be a result of the charging effect due to the nonconductive corrosion product layers. The XPS

results indicate that a new layer of $CaCO_3$ was formed when specimen was immersed in solution prepared with tap water, which is in good agreement with the cross-sectional element mappings.

According to the XRD results shown in Fig. 12, the corrosion products of alloys immersed in solution prepared with deionized water mainly consisted of $Mg(OH)_2$. Nevertheless, when alloys were immersed in solution prepared with tap water, the corrosion products became much more complex and $CaCO_3$ in different crystalline polymorphs turned out to be the main corrosion products besides $Mg(OH)_2$. For Mg0.5Zn and Mg0.5Zn0.2Ge alloys, calcite and aragonite were the main forms of $CaCO_3$, while with increasing content of Ca in the bulk alloy, aragonite was absent but a new $CaCO_3$, vaterite, was formed on the alloy surface instead. Combining Fig. 7 with Fig. 12b, we can conclude that the regular cubic crystals were calcite, the flower-like corrosion products were aragonite and the pyramid products were vaterite. No evidence of magnesium carbonate components were detected. The small diffraction peak of $Mg_2Ge$ should come from the second phases in Mg0.5Zn0.2Ge alloy. The composition of the corrosion products determined by XRD, XPS and element mapping results were in good agreement.

**4. Discussion**

Mg and its alloys are intrinsically susceptibility to corrosion in aqueous environment due to the low thermodynamic stability [31]. When Mg is immersed in NaCl solution, corrosion initiates as:

$$Mg\ (s) \rightarrow Mg^{2+}\ (aq) + 2e^- \quad (1)$$

Simultaneously, the most important cathodic reactions are water and oxygen reduction [32]:

$$2H_2O\ (aq) + 2e^- \rightarrow 2OH^-\ (aq) + H_2\ (g) \quad (2)$$

$$O_2\ (g) + 2H_2O\ (aq) + 4e^- \rightarrow 4OH^-\ (aq) \quad (3)$$

Following that, the metallic cations react with the hydroxyl ions forming insoluble precipitates:

$$Mg^{2+}(aq) + 2OH^{-}(aq) \rightarrow Mg(OH)_2(s) \quad (4)$$

The dissolution of Mg results in an increase of pH near the substrate surface and evolution of hydrogen bubbles. Subsequently, $Mg(OH)_2$ quickly precipitates on the alloy surface forming the primary corrosion product layer. Formation of magnesium carbonate components is possible at the presence of $CO_2$ [33-35]. However, in this study, no clear evidence of magnesium carbonate components were found, which was in accordance with the results reported by Pardo et al. and Xin et al. [15, 36]. In the presence of $Cl^-$ ions, local breakdown of the corrosion products layer can occur, resulting in the exposure of the underneath substrate to the corrosive electrolyte. Due to the different bulk compositions and microstructures of Mg0.5Zn, Mg0.5Zn0.5Ca and Mg0.5Zn0.2Ge alloys, the corrosion behavior of the three alloys exhibited some differences in 0.9 *wt.*% NaCl solution prepared with deionized water. Mg0.5Zn and Mg0.5Zn0.5Ca alloys were corrosion-resistant in 0.9 *wt.*% NaCl solution, which led to well-defined capacitive loops in EIS measurements. The simultaneous formation and dissolution of $Mg(OH)_2$ gave rise to fluctuating impedance values. In comparison, the Mg0.5Zn0.2Ge alloy was less corrosion-resistant in 0.9 *wt.*% NaCl solution. Local breakdown of the corrosion products layer happened due to the presence of aggressive $Cl^-$ ions and thus active dissolution of the alloy happened through the defects of the corrosion products film, as revealed by suddenly decreasing impedance values and the less-refined capacitive loop at middle frequency of the impedance spectra after several hours of immersion. With prolonged immersion, the formation of corrosion products suppressed the localized active dissolution of the alloy and thus the impedance spectra revealed two well-defined capacitive loops again.

In 0.9 *wt.*% NaCl solution prepared with tap water, cases were different due to the presence of $Ca^{2+}$. As mentioned above, when Mg alloys are immersed in corrosive electrolyte and corrosion occurs, the concentrations of $Mg^{2+}$ and pH at the alloy/solution interface increase because of the corrosion process. $CO_2$ in the air can dissolve into the solution to some extent and combine with $H_2O$ to form carbonic acid ($H_2CO_3$) which is a well-known weak acid and dissociates as bicarbonate ($HCO_3^-$) ions. When the interfacial pH increased due to the corrosion of the alloys, a conversion of $HCO_3^-$ ions to carbonate ($CO_3^{2-}$) ions took place. The two-step dissociation at higher pH values will also lead to further increase of $CO_2$ solubility in the electrolyte. As a result of interaction with carbonate anion, $CaCO_3$ crystallized as a new corrosion product covering the top of the primary $Mg(OH)_2$ layer. $CaCO_3$ can exist in three anhydrous crystalline phases, that is, calcite, aragonite and vaterite. Among them, calcite is thermodynamically more stable, followed by aragonite and vaterite is the least stable form [25, 37]. The solubility product constants ($K_{sp}$) of calcite, aragonite and vaterite are $3.36 \times 10^{-9}$, $4.6 \times 10^{-9}$ and $1.2 \times 10^{-8}$, respectively, which are lower than that of $MgCO_3$ ($6.82 \times 10^{-6}$) [25, 38]. Thus, $CaCO_3$ was precipitated preferably instead of $MgCO_3$ and the calcite form of $CaCO_3$ was the predominate compound in the corrosion products of the three alloys after immersion in 0.9 *wt.*% NaCl solution prepared with tap water. However, $Mg^{2+}$ have been proved to promote the aragonite form of $CaCO_3$ [39, 40] and the dissolution of the alloys in the present study can provide sufficient $Mg^{2+}$ at the alloy/solution interface, which should account for the presence of aragonite flowers on the surfaces of Mg0.5Zn and Mg0.5Zn0.2Ge alloys. Nevertheless, at the same time, $Mg^{2+}$ also precipitated as $Mg(OH)_2$ ($K_{sp} = 5.61 \times 10^{-12}$) due to the high pH at the alloy/solution interface [25], which largely suppressed the accelerating effect of $Mg^{2+}$ on the formation of aragonite [41]. As a result, the $CaCO_3$ corrosion products on the surfaces of Mg0.5Zn and Mg0.5Zn0.2Ge alloys after immersion in NaCl solution prepared with tap water were predominated by calcite and

accompanied by some aragonite. Compared with Mg0.5Zn and Mg0.5Zn0.2Ge alloys, the higher content of Ca in the Mg0.5Zn0.5Ca alloy could result in a higher concentration of $Ca^{2+}$ at the alloy/solution interface during immersion in corrosive electrolyte. High $Ca^{2+}$ concentration has been reported to promote the formation of vaterite [42]. Moreover, the much higher cathodic current density on the polarization curve of Mg0.5Zn0.5Ca alloy in solution prepared with tap water can lead to higher pH at the metal /solution interface. Therefore, these can be the reasons that vaterite instead of aragonite was present as another $CaCO_3$ crystalline form on Mg0.5Zn0.5Ca alloy surface. As the immersion time increased, the $CaCO_3$-covered area on the surfaces of the alloys gradually increased and finally, a continuous calcite/aragonite $CaCO_3$ corrosion products layer was formed on the top of the $Mg(OH)_2$ products layer except for the Mg0.5Zn0.5Ca alloy. This accounts for the gradually increased impedance of the alloys in NaCl solution prepared with tap water. The non-continuous $CaCO_3$ layer of Mg0.5Zn0.5Ca alloy may be due to the lower stability and higher $K_{sp}$ of vaterite and was responsible for the relatively lower impedance of Mg0.5Zn0.5Ca alloy in solution prepared with tap water. According to the elemental mapping and XPS results, the existence of Zn in the $CaCO_3$ layer can be a result of the incorporation of $Zn^{2+}$ ions into the precipitation of $CaCO_3$ [43, 44].

The mechanisms of the formation of different corrosion products in the two different corrosive media are schematically depicted in Fig. 13. The formation process was also investigated by examining the surface morphologies after immersion in solutions for different durations as shown in Fig. 14 with Mg0.5Zn alloy as representative. In solution prepared with deionized water, the corrosion product film gradually thickened with increasing immersion time as indicated by the gradually invisible grain boundaries underneath the corrosion products and scratches resulting from the grinding process as well as the appearance of cracks. In solution prepared with tap water, when the alloy was immersed for only 10 min, the

corroded morphology was similar to the case in solution prepared with deionized water, characterized by a thin corrosion product layer with some segregations of $Mg(OH)_2$. However, with prolonged immersion, regularly shaped cubic (denoted by red dashed circles) and flower-like (denoted by yellow dashed circles) $CaCO_3$ crystallites were formed on the surface and the coverage of the primary corrosion product layer by the secondary $CaCO_3$ layer gradually increased with exposure time. The remained signs of scratches in Fig. 6, Fig. 7 and Fig. 14 as well as the shallow corroded cavities and stilts of non-corroded bulk materials in Fig. 8 indicated that the primary $Mg(OH)_2$ layer grew predominately adjacent to the bulk material, i.e., from the initial surface (external surface) towards the internal bulk material. This phenomenon has been reported in the work of Kalb et al. [38] by observing the temporal evolution of bulk erosion and corrosion layer formation. In comparison, $Ca^{2+}$ and $HCO_3^-/CO_3^{2-}$ diffused from the electrolyte towards the material surface and deposited on the primary $Mg(OH)_2$ layer surface, in which process the $Mg(OH)_2$ served as a nucleus for the deposition of $CaCO_3$. The increased pH resulting from the dissolution of Mg can drive the equilibrium between $HCO_3^-$ and $CO_3^{2-}$ shifting strongly towards carbonates near the alloy surface, which in turn favored the precipitation of $CaCO_3$. Additionally, as indicated by the corrosion products formation process in Figure 14, a relatively compact $CaCO_3$ was already formed after immersion for 6 h in solution prepared with tap water, which can block the ions diffusion ($Mg^{2+}$ from interior towards exterior and $Ca^{2+}$ from exterior towards interior). As a result, an apparent two-layer cross section morphology was formed. Small amount of other ions (sulfate, fluoride etc.) also existed in the tap water and may affect the formation of corrosion products. For example, sulfate has been demonstrated to favor the transformation from calcite to aragonite [39] but the effects of other trace ions on the crystalline of $CaCO_3$ remain to be considered but seem to be not very effective. The typical flower-like morphology of aragonite was present in this study, while the typical rhombohedral

appearance of calcite and spherical or hexagonal shapes of vaterite were absent and replaced by cubic calcite and pyramid shaped vaterite, which may be due to the complex composition of the tap water used here and the labile metal/solution interface during the immersion of those alloys [45].

In summary, our study showed that the purity of water used for solution preparation had a significant influence on the corrosion resistance of Mg alloys. When Mg alloys were immersed in testing media prepared with deionized water, only partially protective $Mg(OH)_2$ corrosion products layer was formed on the Mg alloys surfaces. When non-deionized water rich in $Ca^{2+}$ was used to prepare the testing medium, a new corrosion products layer composed of different crystalline phases of $CaCO_3$ was formed covering the top of the $Mg(OH)_2$ layer, which contributed to one order of magnitude higher corrosion resistance of the alloy compared with that tested in solution prepared with deionized water. Besides, the higher content of Ca in the alloy can affect the crystalline structure of $CaCO_3$ in the corrosion products. What needs to be pointed out here is that, as introduced above, the mutual influence of ions in solution can differ from the individual influence of a specific ion, thus the influence of tap water on the corrosion behavior of Mg alloys may be different when the amount of certain ions varies much.

## 5. Conclusions

In this study, the influence of the purity of water used for solution preparation on the corrosion property evaluation of Mg0.5ZnX alloys was investigated. Expectedly, $Mg(OH)_2$ corrosion products layer with limited corrosion protection function was predominately formed on the Mg0.5Zn, Mg0.5Zn0.5Ca and Mg0.5Zn0.2Ge alloys surfaces after immersion in 0.9 *wt.*% NaCl solution prepared with deionized water. Interestingly, when tap water was used for solution preparation, the corrosion resistance of the alloys was improved by almost one order of magnitude according to the electrochemical tests results, which was attributed to

the formation of an additional $CaCO_3$ corrosion product layer on top of the $Mg(OH)_2$ corrosion product layer because of the relatively high content of $Ca^{2+}$ in tap water. The thermodynamically stable calcite form of $CaCO_3$ was predominating in the $CaCO_3$ layer. Besides, aragonite form of $CaCO_3$ was also present on the surfaces of Mg0.5Zn and Mg0.5Zn0.2Ge alloys due to the promotion effect of $Mg^{2+}$, while for Mg0.5Zn0.5Ca alloy, the least stable vaterite was formed instead of aragonite because of the higher Ca content in the alloy.

More importantly, our results highlight the importance of the electrolyte chosen for evaluating the corrosion resistance of Mg alloys. Particularly, the typical lab practice of using deionized water for corrosive electrolyte may lead to overestimation of the corrosion rates of Mg alloys in comparison to in the service conditions where different cations including $Ca^{2+}$ are present.

**Declarations of interest**

The authors declare that there is no confliction of interest.

**Data availability**

The raw/processed data required to reproduce these findings cannot be shared at this time as the data also forms part of an ongoing study.

**Acknowledgement**

The technical support of Mr. Ulrich Burmester, Mr. Gert Wiese and Mr. Volker Heitmann during this work is gratefully acknowledged. We also would like to give thanks to Ms. Sabine Schubert for the analysis of the chemical composition of alloys and the colleagues Daniel Proefrock and Kirstin Daehnke from the Institute of Coastal Research at HZG for the analysis of the deionized water. The author P.L. Jiang would like to thank the financial support from China Scholarship Council (CSC).

## Reference


[1] K.W. Guo, A review of magnesium/magnesium alloys corrosion and its protection, Recent Patents on Corrosion Science, 2 (2010) 13-21.
[2] K. Gusieva, C.H.J. Davies, J.R. Scully, N. Birbilis, Corrosion of magnesium alloys: the role of alloying, International Materials Reviews, 60 (2015) 169-194. https://doi.org/10.1179/1743280414Y.0000000046.
[3] J.W. Chang, X.W. Guo, P.H. Fu, L.M. Peng, W.J. Ding, Effect of heat treatment on corrosion and electrochemical behaviour of Mg–3Nd–0.2Zn–0.4Zr (wt.%) alloy, Electrochimica Acta, 52 (2007) 3160-3167. https://doi.org/10.1016/j.electacta.2006.09.069.
[4] E. Ghali, W. Dietzel, K.U. Kainer, General and localized corrosion of magnesium alloys: a critical review, Journal of materials engineering and performance, 13 (2004) 7-23. DOI: 10.1361/10599490417533.
[5] G.L. Song, A. Atrens, Understanding magnesium corrosion—a framework for improved alloy performance, Advanced engineering materials, 5 (2003) 837-858. https://doi.org/10.1002/adem.200310405
[6] Y.C. Xin, C.L. Liu, X.M. Zhang, G.Y. Tang, X.B. Tian, P.K. Chu, Corrosion behavior of biomedical AZ91 magnesium alloy in simulated body fluids, Journal of Materials Research, 22 (2007) 2004-2011. https://doi.org/10.1557/jmr.2007.0233.
[7] R.C. Zeng, Y. Hu, S.K. Guan, H.Z. Cui, E.H. Han, Corrosion of magnesium alloy AZ31: The influence of bicarbonate, sulphate, hydrogen phosphate and dihydrogen phosphate ions in saline solution, Corrosion Science, 86 (2014) 171-182. https://doi.org/10.1016/j.corsci.2014.05.006.
[8] Y. Jang, B. Collins, J. Sankar, Y. Yun, Effect of biologically relevant ions on the corrosion products formed on alloy AZ31B: An improved understanding of magnesium corrosion, Acta biomaterialia, 9 (2013) 8761-8770. https://doi.org/10.1016/j.actbio.2013.03.026.
[9] Y.C. Xin, K.F. Huo, H. Tao, G.Y. Tang, P.K. Chu, Influence of aggressive ions on the degradation behavior of biomedical magnesium alloy in physiological environment, Acta Biomaterialia, 4 (2008). https://doi.org/10.1016/j.actbio.2008.05.014.
[10] D. Mei, S.V. Lamaka, J. Gonzalez, F. Feyerabend, R. Willumeit-Römer, M.L. Zheludkevich, The role of individual components of simulated body fluid on the corrosion behavior of commercially pure Mg, Corrosion Science, 147 (2019) 81-93. https://doi.org/10.1016/j.corsci.2018.11.011.
[11] M. Grabowski, D. Bluecher, M. Korte, S. Virtanen, Influence of $Ca^{2+}$ in Deicing Salt on the Corrosion Behavior of AM50 Magnesium Alloy, Corrosion, 70 (2014) 1008-1023. https://doi.org/10.5006/1268.
[12] M. Grabowski, D. Bluecher, M. Korte, S. Virtanen, The Influence of $Ca^{2+}$ in Deicing Salt on the Chemistry of Corrosion Products Formed on AM50 Magnesium Alloy—Calcareous Deposition, Corrosion, 71 (2015) 703-725. https://doi.org/10.5006/1539.
[13] F. Witte, N. Hort, C. Vogt, S. Cohen, K.U. Kainer, R. Willumeit, F. Feyerabend, Degradable biomaterials based on magnesium corrosion, Current opinion in solid state and materials science, 12 (2008) 63-72. https://doi.org/10.1016/j.cossms.2009.04.001.
[14] Y. Xin, T. Hu, P.K. Chu, In vitro studies of biomedical magnesium alloys in a simulated physiological environment: a review, Acta biomaterialia, 7 (2011) 1452-1459. https://doi.org/10.1016/j.actbio.2010.12.004.
[15] A. Pardo, M.C. Merino, A.E. Coy, R. Arrabal, F. Viejo, E. Matykina, Corrosion behaviour of magnesium/aluminium alloys in 3.5 wt.% NaCl, Corrosion Science, 50 (2008) 823-834. https://doi.org/10.1016/j.corsci.2007.11.005.
[16] Y.W. Song, D.Y. Shan, R.S. Chen, E.H. Han, Corrosion characterization of Mg–8Li alloy in NaCl solution, Corrosion Science, 51 (2009) 1087-1094. https://doi.org/10.1016/j.corsci.2009.03.011.
[17] G. Ben-Hamu, D. Eliezer, K.S. Shin, The role of $Mg_2Si$ on the corrosion behavior of wrought Mg–Zn–Mn alloy, Intermetallics, 16 (2008) 860-867. https://doi.org/10.1016/j.intermet.2008.03.003.
[18] V. Lisitsyn, G. Ben-Hamu, D. Eliezer, K.S. Shin, Some particularities of the corrosion behaviour of Mg–Zn–Mn–Si–Ca alloys in alkaline chloride solutions, Corrosion Science, 52 (2010) 2280-2290. https://doi.org/10.1016/j.corsci.2010.03.017.

[19] J. Zhao, K. Yu, Y.N. Hu, S.J. Li, X. Tan, F.W. Chen, Z.M. Yu, Discharge behavior of Mg–4 wt% Ga–2 wt% Hg alloy as anode for seawater activated battery, Electrochimica Acta, 56 (2011) 8224-8231. https://doi.org/10.1016/j.electacta.2011.06.065.
[20] X. Gao, J.F. Nie, Characterization of strengthening precipitate phases in a Mg–Zn alloy, Scripta Materialia, 56 (2007) 645-648. https://doi.org/10.1016/j.scriptamat.2007.01.006.
[21] L.Y. Wei, G.L. Dunlop, H. Westengen, Precipitation hardening of Mg-Zn and Mg-Zn-RE alloys, Metallurgical and Materials Transactions A, 26 (1995) 1705-1716. https://doi.org/10.1007/BF02670757.
[22] G.L. Song, Control of biodegradation of biocompatable magnesium alloys, Corrosion Science, 49 (2007) 1696-1701. https://doi.org/10.1016/j.corsci.2007.01.001.
[23] Stadtwerke Geesthacht, https://www.stadtwerke-geesthacht.de/wasser.html, 2018 (accessed 23 April 2018).
[24] D.S. Gandel, N. Birbilis, M.A. Easton, M.A. Gibson, Influence of manganese, zirconium and iron on the corrosion of magnesium, Proceedings of corrosion & prevention, (2010) 875-885.
[25] M. Jamesh, S. Kumar, T.S.N. Sankara Narayanan, Corrosion behavior of commercially pure Mg and ZM21 Mg alloy in Ringer's solution–Long term evaluation by EIS, Corrosion Science, 53 (2011) 645-654. https://doi.org/10.1016/j.corsci.2010.10.011.
[26] V.P. Zakaznova-Herzog, H.W. Nesbitt, G.M. Bancroft, J.S. Tse, High resolution core and valence band XPS spectra of non-conductor pyroxenes, Surface science, 600 (2006) 3175-3186. https://doi.org/10.1016/j.susc.2006.06.012.
[27] L.M. Haselbach, S.G. Ma, Potential for carbon adsorption on concrete: Surface XPS analyses, Environmental science & technology, 42 (2008) 5329-5334. DOI: 10.1021/es800717q.
[28] J.W. Jang, C.E. Lee, S.C. Lyu, T.J. Lee, C.J. Lee, Structural study of nitrogen-doping effects in bamboo-shaped multiwalled carbon nanotubes, Applied physics letters, 84 (2004) 2877-2879. https://doi.org/10.1063/1.1697624.
[29] M. Ni, B.D. Ratner, Differentiating calcium carbonate polymorphs by surface analysis techniques—an XPS and TOF-SIMS study, Surface and Interface Analysis, 40 (2008) 1356-1361. https://doi.org/10.1002/sia.2904.
[30] R. Babilas, A. Bajorek, P. Sakiewicz, A. Kania, D. Szyba, Corrosion resistance of resorbable Ca-Mg-Zn-Yb metallic glasses in Ringer's solution, Journal of Non-Crystalline Solids, 488 (2018) 69-78. https://doi.org/10.1016/j.jnoncrysol.2018.02.028.
[31] S. Virtanen, Biodegradable Mg and Mg alloys: Corrosion and biocompatibility, Materials Science and Engineering: B, 176 (2011) 1600-1608. https://doi.org/10.1016/j.mseb.2011.05.028.
[32] E.L. Silva, S.V. Lamaka, D. Mei, M.L. Zheludkevich, The Reduction of Dissolved Oxygen During Magnesium Corrosion, ChemistryOpen, 7 (2018) 664-668. https://doi.org/10.1002/open.201800076.
[33] L. Wang, T. Shinohara, B.-P. Zhang, Corrosion behavior of AZ31 magnesium alloy in dilute sodium chloride solutions, Zairyo-to-Kankyo, 58 (2009) 105-110. https://doi.org/10.3323/jcorr.58.105.
[34] J.S. Liao, M. Hotta, S.-i. Motoda, T. Shinohara, Atmospheric corrosion of two field-exposed AZ31B magnesium alloys with different grain size, Corrosion Science, 71 (2013) 53-61. https://doi.org/10.1016/j.corsci.2013.02.003.
[35] Q. Qu, J. Ma, L. Wang, L. Li, W. Bai, Z.T. Ding, Corrosion behaviour of AZ31B magnesium alloy in NaCl solutions saturated with $CO_2$, Corrosion Science, 53 (2011) 1186-1193. https://doi.org/10.1016/j.corsci.2010.12.014.
[36] R.L. Xin, B. Li, L. Li, Q. Liu, Influence of texture on corrosion rate of AZ31 Mg alloy in 3.5 wt.% NaCl, Materials & Design, 32 (2011) 4548-4552. https://doi.org/10.1016/j.matdes.2011.04.031.
[37] J. Jiang, K. Tauer, Y.H. Qiu, Y.X. Zhong, M.R. Gao, M. Antonietti, S.H. Yu, Thermosensitive polymer controlled morphogenesis and phase discrimination of calcium carbonate, Chemical Communications, 53 (2017) 6464-6467. DOI: 10.1039/C7CC02684F.
[38] H. Kalb, A. Rzany, B. Hensel, Impact of microgalvanic corrosion on the degradation morphology of WE43 and pure magnesium under exposure to simulated body fluid, Corrosion Science, 57 (2012) 122-130. https://doi.org/10.1016/j.corsci.2011.12.026.

[39] J.L. Bischoff, W.S. Fyfe, Catalysis, inhibition, and the calcite-aragonite problem;[Part] 1, The aragonite-calcite transformation, American Journal of Science, 266 (1968) 65-79. DOI: 10.2475/ajs.266.2.65.
[40] F.C. Meldrum, S.T. Hyde, Morphological influence of magnesium and organic additives on the precipitation of calcite, Journal of Crystal Growth, 231 (2001) 544-558. https://doi.org/10.1016/S0022-0248(01)01519-6.
[41] J.L. Bischoff, Catalysis, inhibition, and the calcite-aragonite problem;[Part] 2, The vaterite-aragonite transformation, American Journal of Science, 266 (1968) 80-90. DOI: 10.2475/ajs.266.2.80.
[42] H. Roques, A. Girou, Kinetics of the formation conditions of carbonate tartars, Water Research, 8 (1974) 907-920. https://doi.org/10.1016/0043-1354(74)90105-5.
[43] A. Glasner, D. Weiss, The crystallization of calcite from aqueous solutions and the role of zinc and magnesium ions—I. Precipitation of calcite in the presence of $Zn^{2+}$ ions, Journal of Inorganic and Nuclear Chemistry, 42 (1980) 655-663. https://doi.org/10.1016/0022-1902(80)80210-7.
[44] E.J. Elzinga, R.J. Reeder, X-ray absorption spectroscopy study of $Cu^{2+}$ and $Zn^{2+}$ adsorption complexes at the calcite surface: Implications for site-specific metal incorporation preferences during calcite crystal growth, Geochimica et Cosmochimica Acta, 66 (2002) 3943-3954. https://doi.org/10.1016/S0016-7037(02)00971-7.
[45] C.Y. Tai, F.B. Chen, Polymorphism of $CaCO_3$, precipitated in a constant-composition environment, AIChE Journal, 44 (1998) 1790-1798. https://doi.org/10.1002/aic.690440810.

**Figure captions**

**Fig. 1.** Impedance spectra of (a, b, c) Mg0.5Zn, (d, e, f) Mg0.5Zn0.5Ca and (g, h, i) Mg0.5Zn0.2Ge alloys tested in 0.9 *wt.*% NaCl solution prepared with deionized water for 7 d.

**Fig. 2.** Impedance spectra of (a, b, c) Mg0.5Zn, (d, e, f) Mg0.5Zn0.5Ca and (g, h, i) Mg0.5Zn0.2Ge alloys tested in 0.9 *wt.*% NaCl solution prepared with tap water for 7 d.

**Fig. 3.** Equivalent circuits used to fit the impedance spectra of Mg0.5Zn, Mg0.5Zn0.5Ca and Mg0.5Zn0.2Ge alloys after immersion (a) in 0.9 *wt.*% NaCl solution prepared with deionized water for up to 7 d and in solution prepared with tap water for less than 24 h and (b) in solution prepared with tap water for more than 24 h.

**Fig. 4.** Plots of $R_{sum}$ of Mg0.5Zn, Mg0.5Zn0.5Ca and Mg0.5Zn0.2Ge alloys as a function of immersion time in 0.9 *wt.*% NaCl solutions prepared with (a) deionized and (b) tap water.

**Fig. 5.** Potentiodynamic polarization curves of Mg0.5Zn, Mg0.5Zn0.5Ca and Mg0.5Zn0.2Ge alloys after immersion in 0.9 *wt.*% NaCl solution prepared with deionized or tap water for 7 d.

**Fig. 6.** Surface morphologies of (a, d) Mg0.5Zn, (b,e) Mg0.5Zn0.5Ca and (c,f) Mg0.5Zn0.2Ge alloys after immersion in 0.9 *wt.*% NaCl solution prepared with deionized water.

**Fig. 7.** Surface morphologies of (a, d) Mg0.5Zn, (b, e) Mg0.5Zn0.5Ca and (c, f) Mg0.5Zn0.2Ge alloys after immersion in 0.9 *wt.*% NaCl solution prepared with tap water.

**Fig. 8.** Cross-sectional morphologies of Mg0.5Zn, Mg0.5Zn0.5Ca and Mg0.5Zn0.2Ge alloys after immersion in 0.9 *wt.*% NaCl solutions prepared with deionized and tap water.

**Fig. 9.** SEM images and chemical element mappings of the cross sections of Mg0.5Zn alloy after immersion in 0.9 *wt.*% NaCl solutions prepared with deionized and tap water.

**Fig. 10.** Comparison of XPS survey spectra for Mg0.5Zn surface after immersion in 0.9 *wt.*% NaCl solutions prepared with (a) deionized water and (b) tap water for 6 h (after 1800 s Ar etching).

**Fig. 11.** High resolution region spectra of C 1s and Ca 2s peaks for Mg0.5Zn alloy after immersion in 0.9 *wt.*% NaCl solutions prepared with (a, b) deionized water and tap water (c, d) for 6 h (after 1800 s Ar etching).

**Fig. 12.** XRD patterns for Mg0.5Zn, Mg0.5Zn0.5Ca and Mg0.5Zn0.2Ge alloys after immersion in 0.9 *wt.*% NaCl solutions prepared with (a) deionized and (b) tap water for 7 d.

**Fig. 13.** Schematic presentation of the corrosion processes of the studied alloys in 0.9 *wt.*% NaCl solutions prepared with deionized water and tap water.

**Fig. 14.** Surface morphologies of Mg0.5Zn alloy after immersion in 0.9 *wt.*% NaCl solutions prepared with deionized water and tap water for different durations.

**Figure 1**

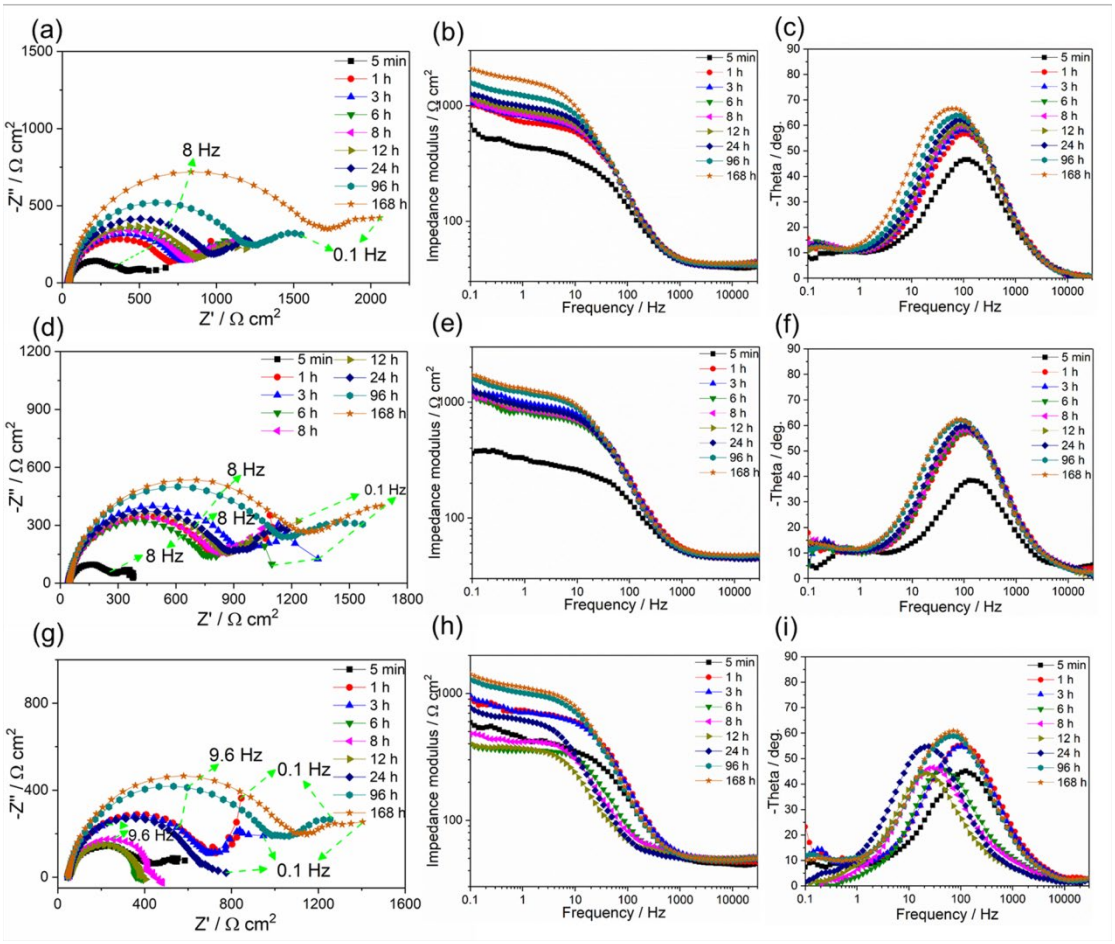
(a)
(b)
(c)
(d)
(e)
(f)
(g)
(h)
(i)
-Z'' / Ω cm2
Z' / Ω cm2
Impedance modulus / Ω cm2
-Theta / deg.
Frequency / Hz
5 min
1 h
3 h
6 h
8 h
12 h
24 h
96 h
168 h
8 Hz
0.1 Hz
9.6 Hz

**Figure 2**

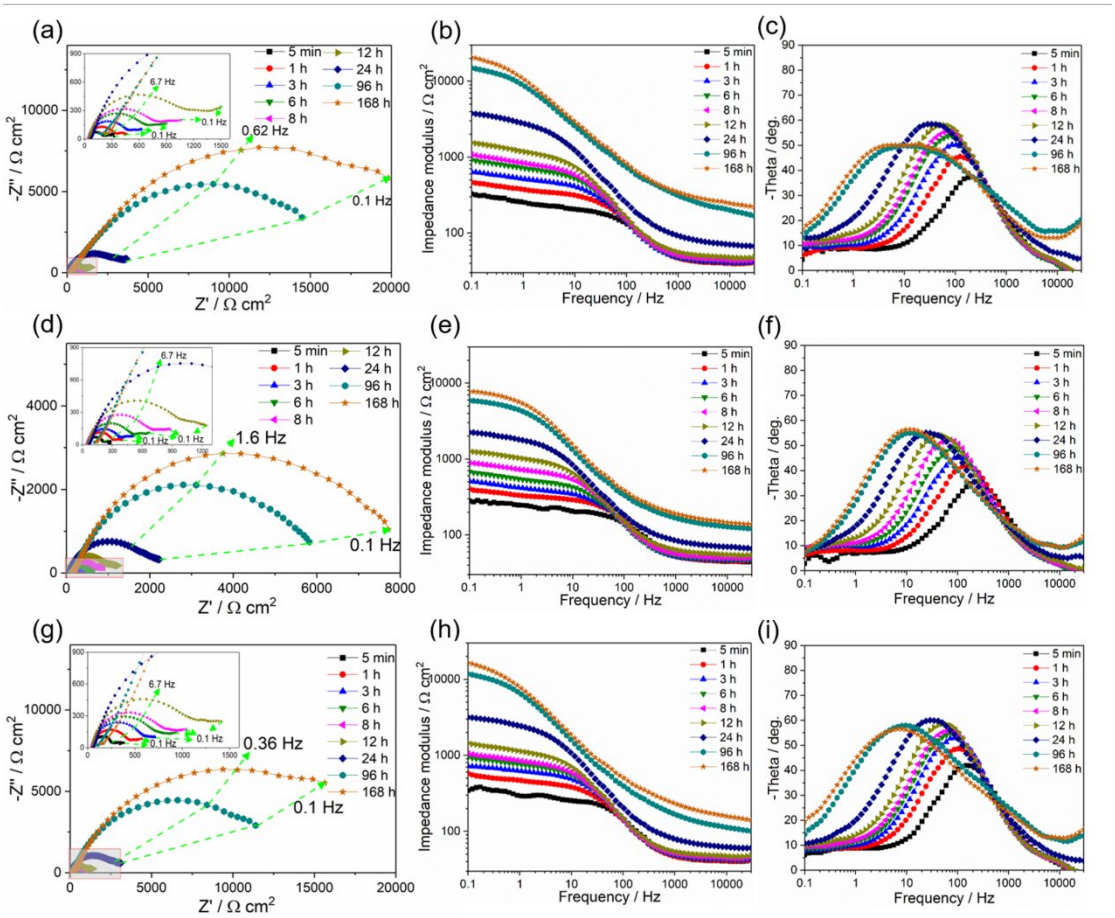
(a)
(b)
(c)
(d)
(e)
(f)
(g)
(h)
(i)
-Z'' / Ω cm2
Z' / Ω cm2
Impedance modulus / Ω cm2
-Theta / deg.
Frequency / Hz
5 min
1 h
3 h
6 h
8 h
12 h
24 h
96 h
168 h
6.7 Hz
0.1 Hz
0.62 Hz
1.6 Hz
0.36 Hz

**Figure 3**

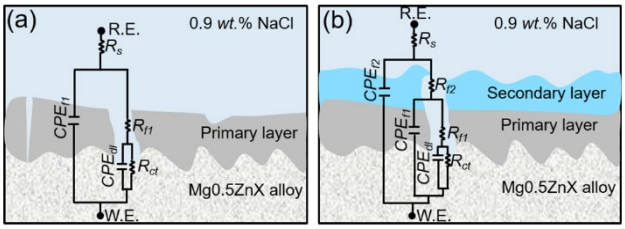
(a)
R.E.
$R_s$
0.9 *wt.*% NaCl
$CPE_{f1}$
$R_{f1}$
Primary layer
$CPE_{dl}$
$R_{ct}$
Mg0.5ZnX alloy
W.E.
(b)
R.E.
$R_s$
0.9 *wt.*% NaCl
$CPE_{f2}$
$R_{f2}$
Secondary layer
$CPE_{f1}$
$R_{f1}$
Primary layer
$CPE_{dl}$
$R_{ct}$
Mg0.5ZnX alloy
W.E.

**Figure 4**

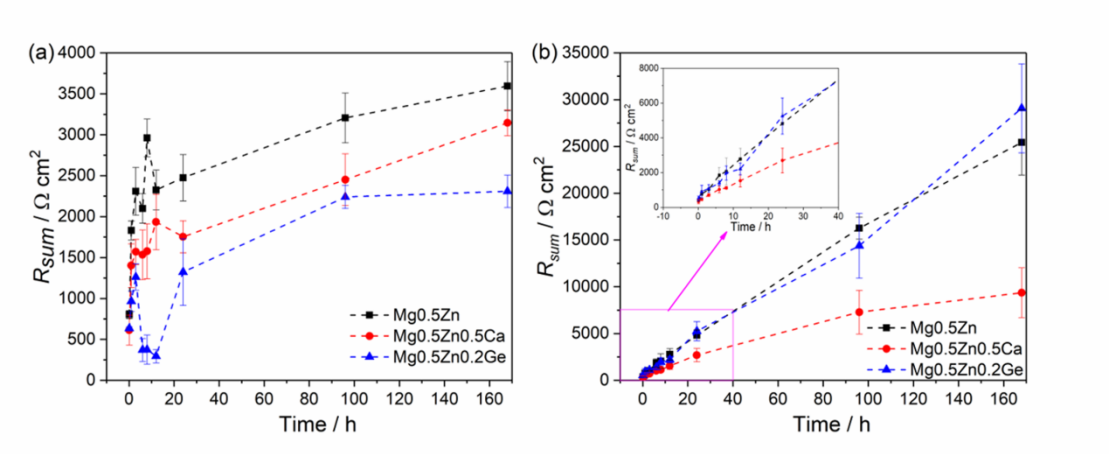

**Figure 5**

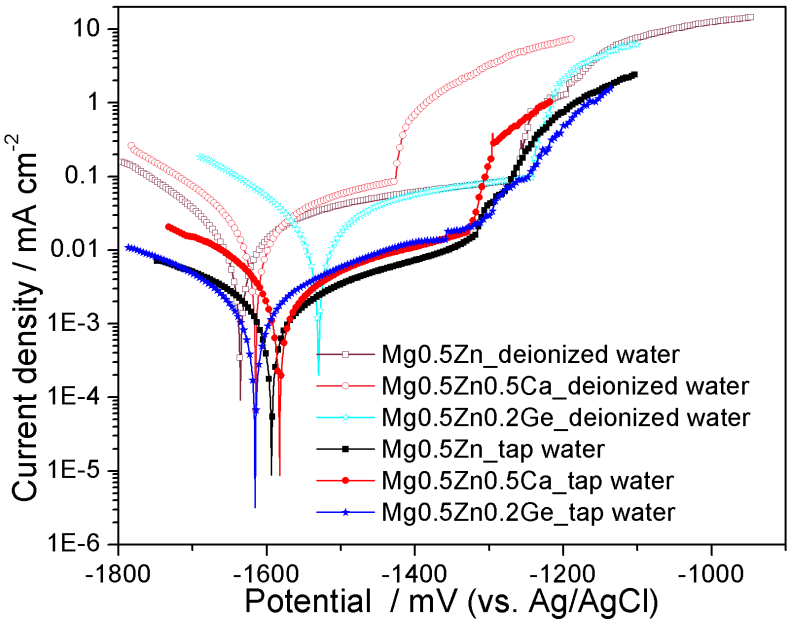
Current density / mA cm-2
10
1
0.1
0.01
1E-3
1E-4
1E-5
1E-6
-1800
-1600
-1400
-1200
-1000
Potential / mV (vs. Ag/AgCl)
Mg0.5Zn_deionized water
Mg0.5Zn0.5Ca_deionized water
Mg0.5Zn0.2Ge_deionized water
Mg0.5Zn_tap water
Mg0.5Zn0.5Ca_tap water
Mg0.5Zn0.2Ge_tap water

**Figure 6**

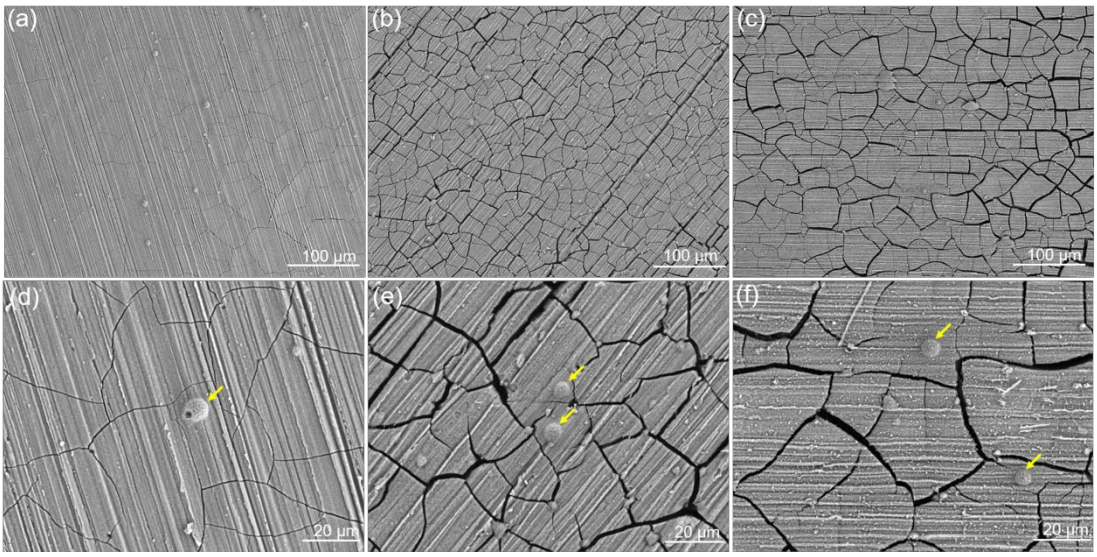

**Figure 7**

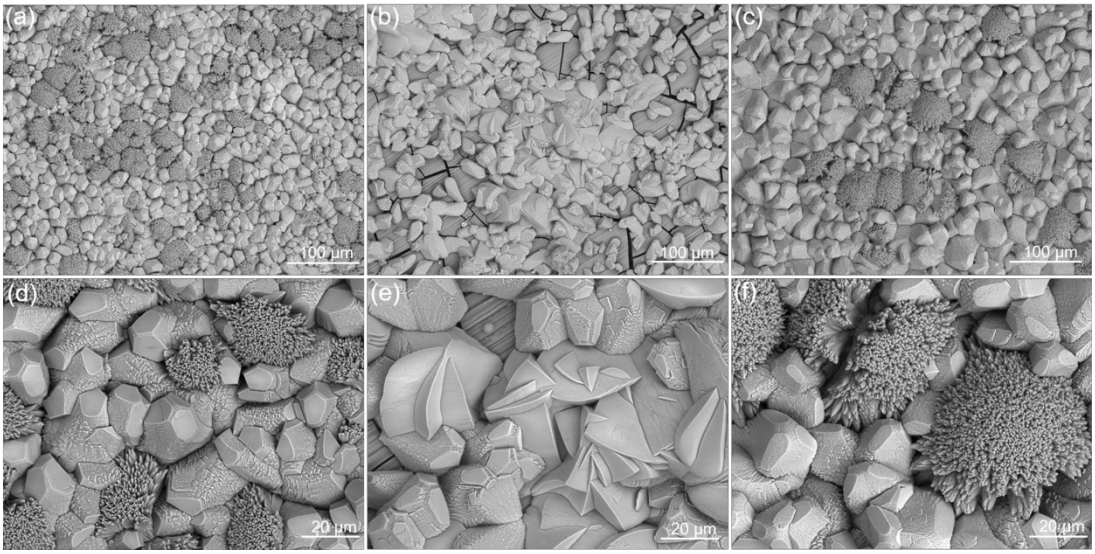

**Figure 8**

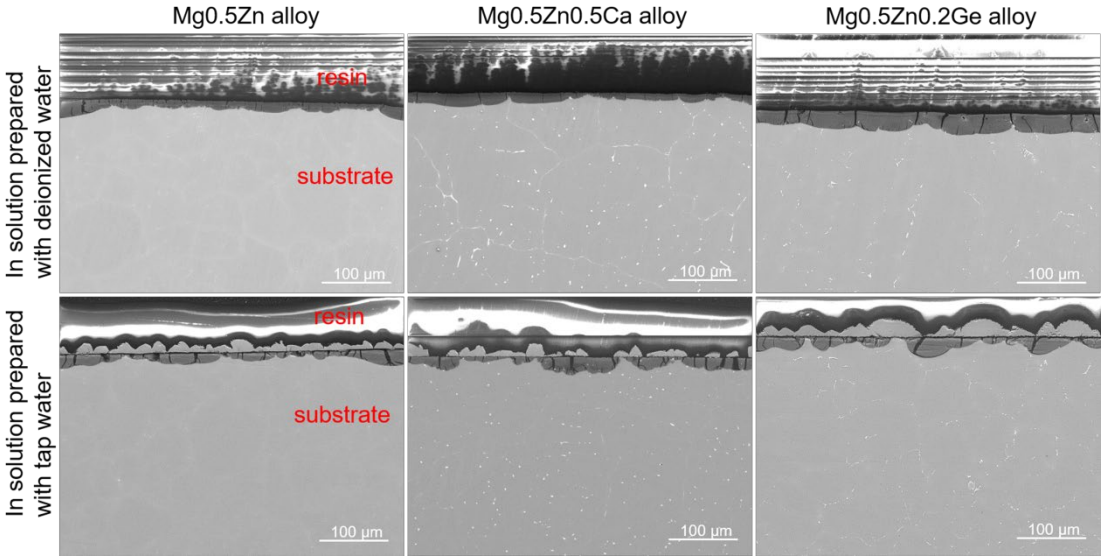
Mg0.5Zn alloy
Mg0.5Zn0.5Ca alloy
Mg0.5Zn0.2Ge alloy
In solution prepared with deionized water
In solution prepared with tap water
resin
substrate
100 μm

**Figure 9**

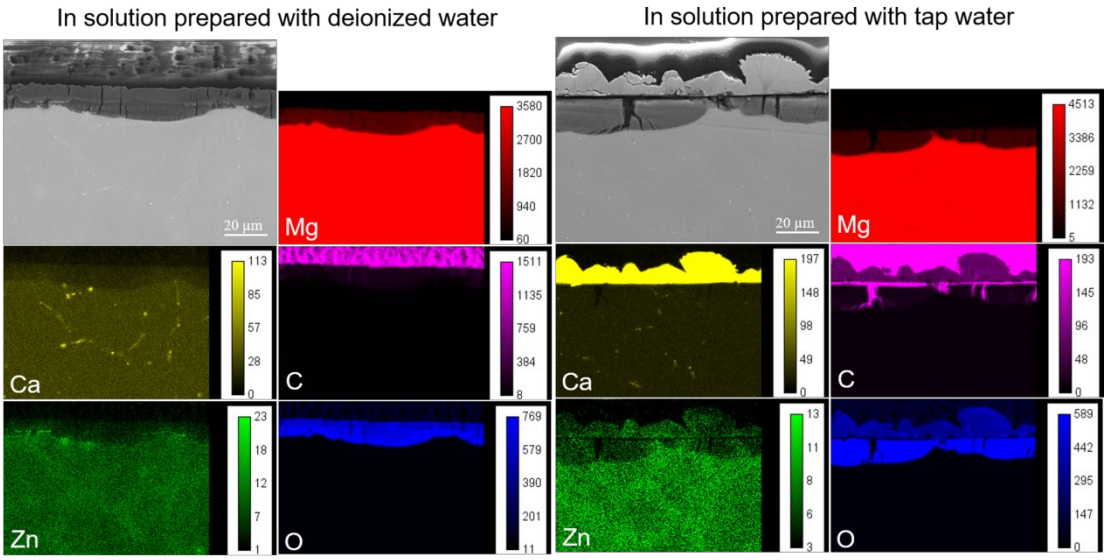
In solution prepared with deionized water
In solution prepared with tap water
20 µm
Mg
Ca
C
Zn
O
3580
2700
1820
940
60
4513
3386
2259
1132
5
113
85
57
28
0
1511
1135
759
384
8
197
148
98
49
0
193
145
96
48
0
23
18
12
7
1
769
579
390
201
11
13
11
8
6
3
589
442
295
147
0

**Figure 10**

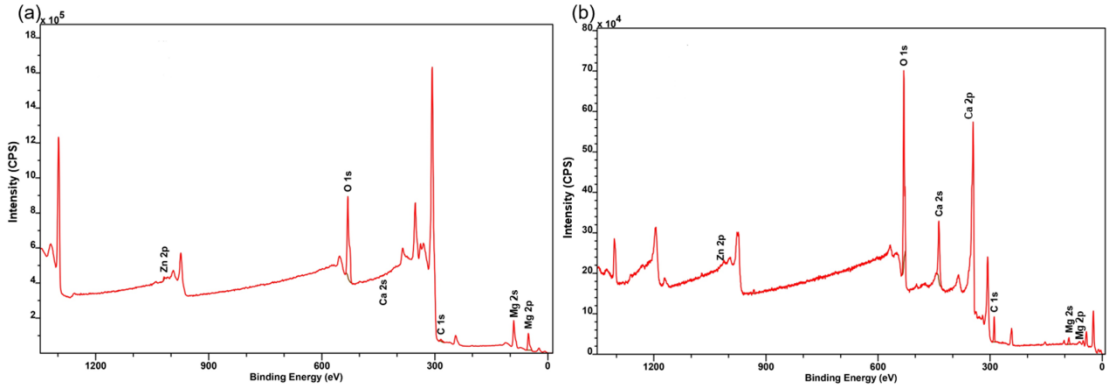
(a)
x 10^5
Intensity (CPS)
Zn 2p
O 1s
Ca 2s
C 1s
Mg 2s
Mg 2p
Binding Energy (eV)
(b)
x 10^4
Intensity (CPS)
O 1s
Ca 2p
Ca 2s
Zn 2p
C 1s
Mg 2s
Mg 2p
Binding Energy (eV)

**Figure 11**

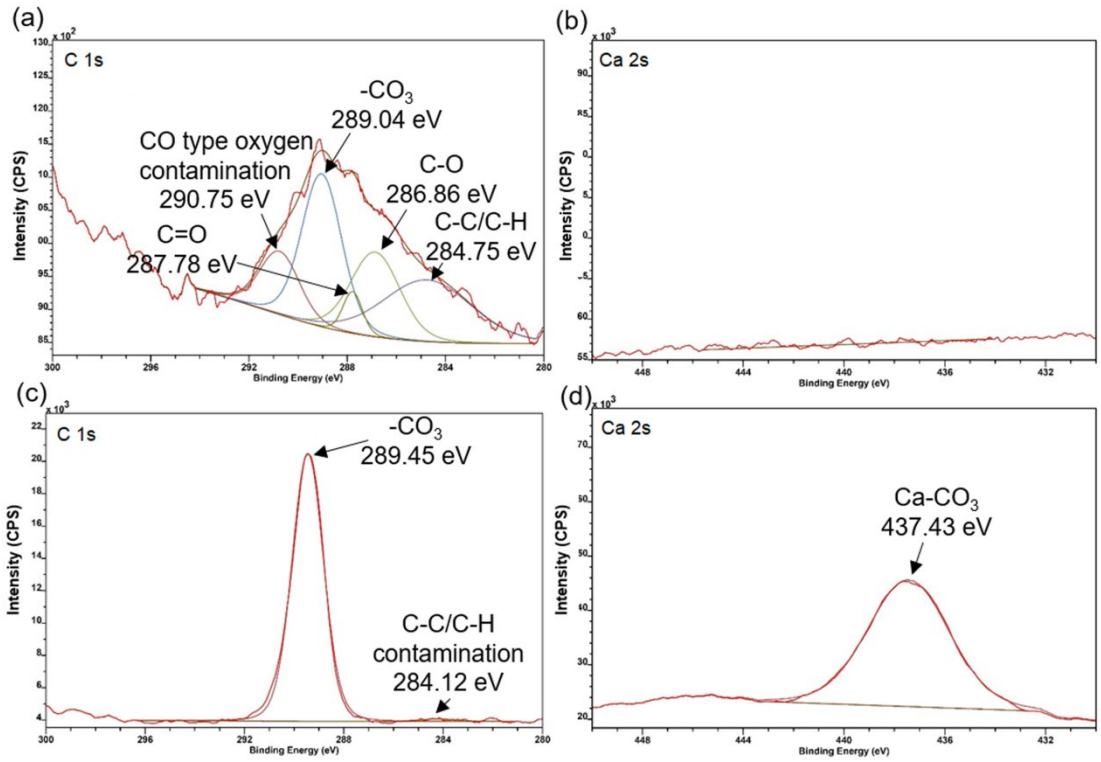
(a)
C 1s
-CO3
289.04 eV
CO type oxygen
contamination
290.75 eV
C-O
286.86 eV
C=O
287.78 eV
C-C/C-H
284.75 eV
Intensity (CPS)
Binding Energy (eV)
(b)
Ca 2s
Intensity (CPS)
Binding Energy (eV)
(c)
C 1s
-CO3
289.45 eV
C-C/C-H
contamination
284.12 eV
Intensity (CPS)
Binding Energy (eV)
(d)
Ca 2s
Ca-CO3
437.43 eV
Intensity (CPS)
Binding Energy (eV)

**Figure 12**

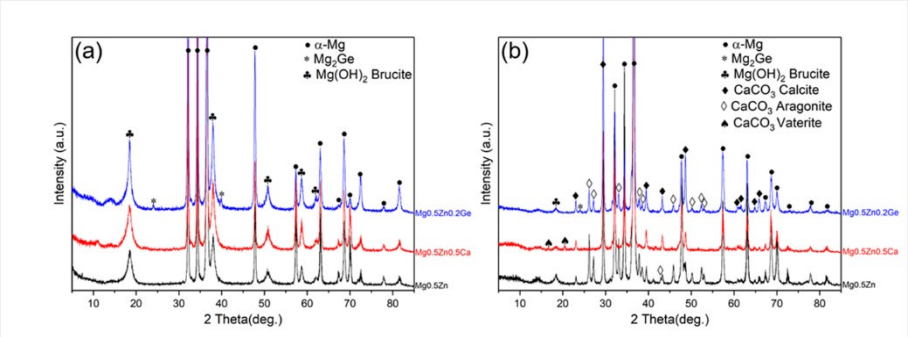
(a)
• α-Mg
* $Mg_2Ge$
♣ $Mg(OH)_2$ Brucite
Intensity (a.u.)
Mg0.5Zn0.2Ge
Mg0.5Zn0.5Ca
Mg0.5Zn
10 20 30 40 50 60 70 80
2 Theta(deg.)
(b)
• α-Mg
* $Mg_2Ge$
♣ $Mg(OH)_2$ Brucite
♦ $CaCO_3$ Calcite
◊ $CaCO_3$ Aragonite
▲ $CaCO_3$ Vaterite
Intensity (a.u.)
Mg0.5Zn0.2Ge
Mg0.5Zn0.5Ca
Mg0.5Zn
10 20 30 40 50 60 70 80
2 Theta(deg.)

**Figure 13**

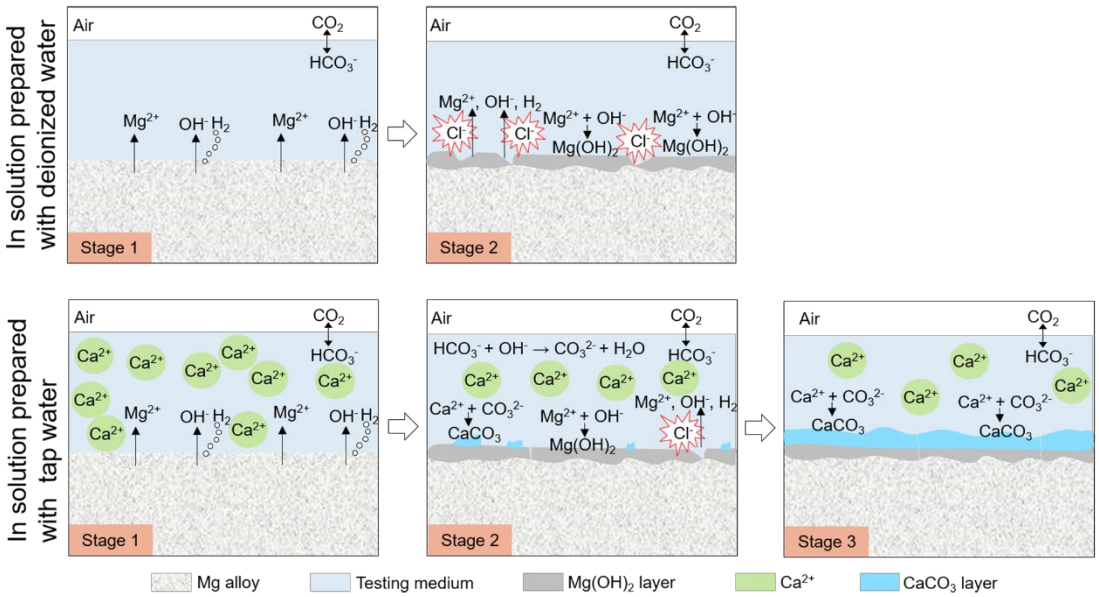
In solution prepared with deionized water
In solution prepared with tap water
Air
$CO_2$
$HCO_3^-$
$Mg^{2+}$
$OH^-$
$H_2$
$Ca^{2+}$
$Cl^-$
$Mg(OH)_2$
$CaCO_3$
$HCO_3^- + OH^- \rightarrow CO_3^{2-} + H_2O$
$Ca^{2+} + CO_3^{2-}$
Stage 1
Stage 2
Stage 3
Mg alloy
Testing medium
$Mg(OH)_2$ layer
$Ca^{2+}$
$CaCO_3$ layer

**Figure 14**

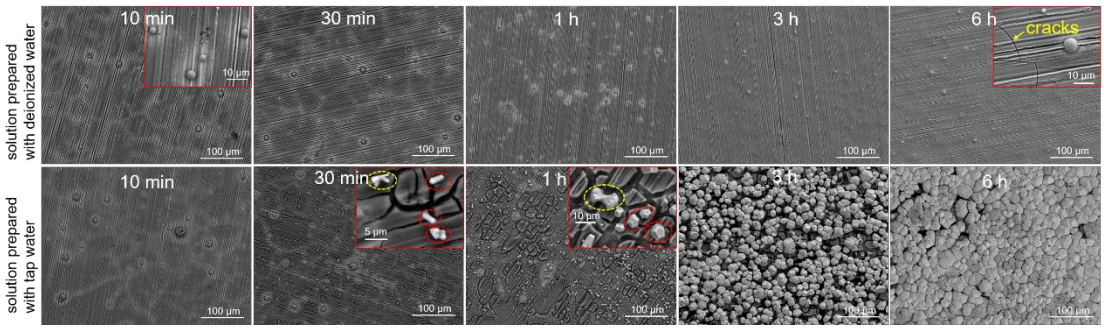
solution prepared with deionized water
10 min
30 min
1 h
3 h
6 h
cracks
solution prepared with tap water
10 min
30 min
1 h
3 h
6 h

**Tables**

**Table 1.** Chemical compositions of the alloys used in this study.

| Alloys | Element (*wt.*%) | | | | | | | | | |
|---|---|---|---|---|---|---|---|---|---|---|
| | Ca | Ge | Zn | Fe | Cu | Ni | Mn | Si | Ag | Al |
| Mg0.5Zn | 0.027 | - | 0.457 | 0.00714 | 0.00137 | 0.00067 | 0.0335 | 0.033 | <0.00010 | <0.0100 |
| Mg0.5Zn0.5Ca | 0.41 | - | 0.477 | 0.00351 | 0.00122 | 0.00049 | 0.0341 | 0.0252 | <0.00010 | <0.0100 |
| Mg0.5Zn0.2Ge | 0.0076 | 0.22 | 0.509 | 0.00292 | 0.00144 | 0.00073 | 0.0361 | 0.0363 | <0.00010 | 0.0107 |

**Table 2.** Parameters of deionized and tap water.

| Parameters | Deionized water (RO)* | Tap water [23] |
|---|---|---|
| Conductivity / (µS/cm) | 3.15 | 486 |
| pH | 7.75 | 7.48 |
| Hardness / (°dH) | - | 9.8 |
| Iron / (mg/L) | 0.002 | < 0.115 |
| Ammonium / (mg/L) | 0.00000722 | < 0.05 |
| Nitrite / (mg/L) | - | < 0.01 |
| Nitrate / (mg/L) | - | < 1.0 |
| Chloride / (mg/L) | - | 11 |
| Sulfate / (mg/L) | - | 12 |
| Calcium / (mg/L) | - | 59 |
| Magnesium / (mg/L) | - | 5.5 |
| Sodium / (mg/L) | - | 6.9 |
| Fluoride / (mg/L) | - | 0.21 |
| Palladium / (mg/L) | 0.001 | |
| Silicon / (µmol/L) | 0.07 | |
| Phosphate / (µmol/L) | 0.03 | |
| $NO_x$ / (µmol/L) | 0.14 | |

* Ion concentrations were determined by atom absorption spectroscopy (AAS) or ion chromatography

**Table 3.** Fitting parameters of the potentiodynamic polarization curves of Mg0.5Zn, Mg0.5Zn0.5Ca and Mg0.5Zn0.2Ge alloys after immersion in 0.9 *wt.*% NaCl solution prepared with deionized or tap water for 7 d.

| Medium | Alloy | Intercept *CR* / mm year$^{-1}$ | Intercept $i_{corr}$ / mA cm$^{-2}$ | $E_{corr}$ / mV | $E_{bd}$ / mV |
|---|---|---|---|---|---|
| Solution prepared with deionized water | Mg0.5Zn | 0.22 ± 0.04 | 0.010 ± 0.002 | -1655 ± 17 | -1255 ± 51 |
| | Mg0.5Zn0.5Ca | 0.28 ± 0.01 | 0.012 ± 0.001 | -1598 ± 17 | -1358 ± 48 |
| | Mg0.5Zn0.2Ge | 0.29 ± 0.02 | 0.013 ± 0.001 | -1566 ± 29 | -1194 ± 35 |
| Solution prepared with tap water | Mg0.5Zn | 0.025 ± 0.002 | 0.001 ± 0.0001 | -1594 ± 4 | -1298 ± 20 |
| | Mg0.5Zn0.5Ca | 0.044 ± 0.009 | 0.002 ± 0.0004 | -1564 ± 12 | -1354 ± 40 |
| | Mg0.5Zn0.2Ge | 0.024 ± 0.005 | 0.001 ± 0.0002 | -1618 ± 27 | -1360 ± 32 |